Spin-Dependent Delocalization in Three Isostructural Complexes $[LFeNiFeL]^{2+/3+/4+}$ (L = 1,4,7-(4-*tert*-Butyl-2-mercaptobenzyl)-1,4,7-triazacyclononane)

Thorsten Glaser,[†] Frank Kesting,[†] Thomas Beissel,[†] Eckhard Bill,[†] Thomas Weyhermüller,[†] Wolfram Meyer-Klaucke,[‡] and Karl Wieghardt*[,†]

Max-Planck-Institut für Strahlenchemie, Stiftstrasse 34-36, D-45470 Mülheim an der Ruhr, Germany, and the European Molecular Biology Laboratory, Outstation Hamburg, D-22603 Hamburg, Germany

Received September 18, 1998

The reaction of mononuclear $[LFe^{III}]$ where L represents the trianionic ligand 1,4,7-tris(4-*tert*-butyl-2-mercaptobenzyl)-1,4,7-triazacyclononane with $NiCl_2 \cdot 6H_2O$ and subsequent oxidations with $[Ni^{III}(tacn)_2](ClO_4)_3$ (tacn = 1,4,7-triazacyclononane) and PbO_2/methanesulfonic acid produced an isostructural series of complexes $[LFeNiFeL]^{n+}$ ($n = 2$ (**1**), $n = 3$ (**2**), $n = 4$ (**3**)), which were isolated as PF_6^- (**1**, **3**) or ClO_4^- salts (**2**). The molecular structures were established by X-ray crystallography for $[LFeNiFeL](ClO_4)_2 \cdot 5CH_3CN$ (**1***), $C_{88}H_{123}Cl_2Fe_2N_{11}NiO_8S_6$, and $[LFeNiFeL](ClO_4)_3 \cdot 8$acetone (**2***), $C_{102}H_{156}Cl_3Fe_2N_6NiO_{20}S_6$. Both compounds crystallize in the triclinic space group $P\bar{1}$ with $a = 13.065(2)$ Å (13.155(2) Å), $b = 13.626(3)$ Å (13.747(3) Å), $c = 14.043(3)$ Å (16.237(3) Å), $\alpha = 114.47(3)°$ (114.20(2)°), $\beta = 97.67(3)°$ (96.57(2)°), $\gamma = 90.34(3)°$ (98.86(2)°), $Z = 1(1)$ (values in parentheses refer to **2***). The cations in **1**, **2**, and **3** have been determined to be isostructural by Fe and Ni K-edge extended X-ray absorption fine structure (EXAFS) spectroscopy. All compounds contain linear trinuclear cations (face-sharing octahedral) with an $N_3Fe(\mu\text{-}SR)_3Ni(\mu\text{-}SR)_3FeN_3$ core structure. The electronic structures of **1**, **2**, and **3** have been studied by Fe and Ni K-edge X-ray absorption near edge (XANES), UV−vis, EPR, and Mössbauer spectroscopy as well as by temperature-dependent magnetic susceptibility measurements. Complexes **1** and **3** possess an $S_t = 0$ whereas **2** has an $S_t = {}^1/_2$ ground state. It is shown that the electronic structures cannot be described by using localized valences (oxidation states). Delocalized models invoking the double-exchange mechanism are appropriate; i.e., spin-dependent delocalization via a double-exchange mechanism yields the correct ground state in each case. **1**, **2**, and **3** represent the first examples where double exchange stabilizes a ground state of *minimum* spin multiplicity.

Introduction

The phenomenon of mixed valency in transition-metal clusters has in recent years attracted considerable scientific activity in both theoretical and synthetic inorganic and bioinorganic chemistry because the description and understanding of their electronic structures pose intellectually challenging problems.[1] Since the early work of Robin and Day in 1967,[2] homonuclear dimers have been classified according to the extent of delocalization of the "additional" electron in $d^n d^{n+1}$ pairs as (i) completely localized (class I) or, alternatively, (ii) completely delocalized (class III) and (iii) an intermediate case (class II) where electron hopping with—in principle—measurable electron transfer rates occurs (class II). Magnetic exchange interactions in homovalent species with deeply trapped local oxidation states are traditionally described by the Heisenberg, Dirac, van Vleck (HDvV) model[1c] by using a spin Hamiltonian $H = -2JS_1 \cdot S_2$ where J is the coupling constant with a negative sign for antiparallel (antiferromagnetic) and a positive sign for spin alignment (ferromagnetic) and S_i represent the local spins at the metal ions 1 and 2.

It has been recognized by Zener[3] and Anderson[4] and the concept has been revived by Girerd,[5] Münck,[6] Noodleman,[7] and others more recently that for mixed-valence dinuclear species an additional "double-exchange" resonance coupling interaction exists where "the double-exchange parameter B splits the Heisenberg spin states into symmetric ($E_s = -B(S + {}^1/_2)$) and antisymmetric ($E_a = +B(S + {}^1/_2)$) combinations of wavefunctions, with the 'extra' electron formally on either half of the dimer".[8d] In dinuclear mixed-valence compounds this double-exchange mechanism (resonance delocalization) enforces maxi-

[†] Max-Planck-Institut für Strahlenchemie.
[‡] European Molecular Biology Laboratory.

(1) (a) *Mixed-Valence Compounds*; Brown, D. B., Ed.; NATO ASIS; Series C: Mathematical and Physical Sciences, Vol. 58; D. Reidel Publishing Company: Dordrecht, The Netherlands, 1979. (b) *Mixed-Valency Systems: Applications in Chemistry, Physics and Biology*; Prassides, K., Ed.; NATO ASI Series; Series C: Mathematical and Physical Sciences, Vol. 343; Kluwer: Dordrecht, The Netherlands, 1990. (c) Kahn, O. *Molecular Magnetism*; VCH Publishers: New York, 1993.
(2) Robin, M. B.; Day, P. *Adv. Inorg. Chem. Radiochem.* **1967**, *10*, 247.
(3) Zener, C. *Phys. Rev.* **1951**, *82*, 403.
(4) Anderson, P. W.; Hasegawa, H. *Phys. Rev.* **1955**, *100*, 675.
(5) Blondin, G.; Girerd, J. J. *Chem. Rev.* **1990**, *90*, 1359 and references therein.
(6) (a) Beinert, H.; Holm, R. H.; Münck, E. *Science* **1997**, *277*, 653. (b) Münck, E.; Papaefthymiou, V.; Surerus, K. K.; Girerd, J. J. In *Metals in Proteins*; Que, L., Ed.; ACS Symposium Series: American Chemical Society: Washington, DC, 1988.
(7) (a) Noodleman, L.; Baerends, E. J. *J. Am. Chem. Soc.* **1984**, *106*, 2316. (b) Noodleman, L. *Inorg. Chem.* **1988**, *27*, 3677.
(8) (a) Drüeke, S.; Chaudhuri, P.; Pohl, K.; Wieghardt, K.; Ding, X. Q.; Bill, E.; Sawaryn, A.; Trautwein, A. X.; Winkler, H.; Gurman, S. J. *J. Chem. Soc., Chem. Commun.* **1989**, 59. (b) Ding, X. Q.; Bominaar, E. L.; Bill, E.; Winkler, H.; Trautwein, A. X.; Drüeke, S.; Chaudhuri, P.; Wieghardt, K. *J. Chem. Phys.* **1990**, *92*, 178. (c) Gamelin, D. R.; Bominaar, E. L.; Mathoniére, C.; Kirk, M. L.; Wieghardt, K.; Girerd, J.-J.; Solomon, E. I. *Inorg. Chem.* **1996**, *35*, 4323. (d) Gamelin, D. R.; Bominaar, E. L.; Kirk, M. L.; Wieghardt, K.; Solomon, E. I. *J. Am. Chem. Soc.* **1996**, *118*, 8085.

10.1021/ic9811289 CCC: $18.00
Published on Web 01/28/1999

mum spin-polarization stabilization; i.e., it always results in net ferromagnetic spin alignment. Experimentally, this has been verified for $[L'Fe^{2.5}(\mu\text{-}OH)_3Fe^{2.5}L']^{2+}$ (L′ = 1,4,7-trimethyl-1,4,7-triazacyclononane)[8] and $Fe^{2.5}{}_2S_2$ pairs[9] in 3Fe-4S and 4Fe-4S iron−sulfur proteins for both of which an $S_t = {}^9/_2$ ground state has been established.

On the other hand, Belinskii[10] in 1987 was the first to point out that the double-exchange parameters of *trinuclear* mixed-valent clusters depend on the total and intermediate spins as well as the individual ion spin.[11] The most important conclusion was that the electronic ground state as determined by competing Heisenberg and double exchange can be a state of either maximum spin *or* minimum (or intermediate) spin multiplicity. In this work we present experimental material which verifies this theory.

In a recent paper[12] we have shown for the isostructural linear trinuclear complexes $[LFeMFeL]^{n+}$ where M = Cr^{III}, Co^{III}, or Fe and n = 1+, 2+, or 3+ and L represents the trianion 1,4,7-tris(4-*tert*-butyl-2-mercaptobenzyl)-1,4,7-triazacyclononane that the dicationic species $[LFeCr^{III}FeL]^{2+}$ (**A**), $[LFeCo^{III}FeL]^{2+}$ (**B**), and $[LFeFeFeL]^{2+}$ (**C**) belong to class III (**A**, **C**) or class II (**B**). **A** and **C** containing low-spin configurated iron ions are completely delocalized species with *maximum* spin ground states of $S_t = 2$ (**A**) and $S_t = 1$ (**C**). The excess electron is delocalized over all three metal ions, and a double-exchange mechanism enforces *ferromagnetic* spin alignment in these dications yielding an $S_{t,max}$ ground state. Compound **B** exhibits temperature-dependent electron hopping behavior on the Mössbauer time scale (10^{-7} s). This has been rationalized by the fact that **B** has a low-spin Co^{III} ($t_{2g}{}^6$ in O_h symmetry) configuration in the central position blocking effectively the $a_1\cdots a_1$ delocalization pathway. In contrast, **A** and **C** have a central Cr^{III} (d^3) and a central low-spin Fe^{III} ($t_{2g}{}^5$) ion, respectively, allowing the "excess" electron to freely move via the $a_1\cdots a_1$ pathway over all three metal sites. This is shown in a valence bond description in Scheme 1.

Here we report a similar series of complexes containing a central nickel ion.[13] Three isostructural species $[LFeNiFeL]^{2+/3+/4+}$ (**1**, **2**, and **3**) have been synthesized and spectroscopically characterized by EPR, Mössbauer, XANES, and EXAFS spectroscopy. We established that (i) the trinuclear complexes attain a ground state of *minimum* spin multiplicity (**1**, $S_t = 0$; **2**, $S_t = {}^1/_2$; **3**, $S_t = 0$) and (ii) they are mixed-valent complexes of class III (delocalized).

Results

Syntheses and Characterization. From the reaction mixture of mononuclear $[LFe^{III}]$[14] and $NiCl_2\cdot 6H_2O$ in methanol were obtained red microcrystals of $[LFeNiFeL](PF_6)_2$ (**1**) upon addition of $NaPF_6$. Oxidation of **1** with 1 equiv of $[Ni^{III}(tacn)_2](ClO_4)_3$[15] (tacn = 1,4,7-triazacyclononane) in acetone yields upon addition of $NaClO_4$ violet crystals of $[LFeNiFeL](ClO_4)_3$ (**2**) whereas the reaction of **1** with PbO_2 and methanesulfonic acid in methanol affords upon addition of $NaPF_6$ blue-black crystals of $[LFeNiFeL](PF_6)_4$ (**3**). Complex **3** decomposes slowly at room temperature, even in the solid state. Therefore, the material was stored at 77 K, where it is stable for weeks.

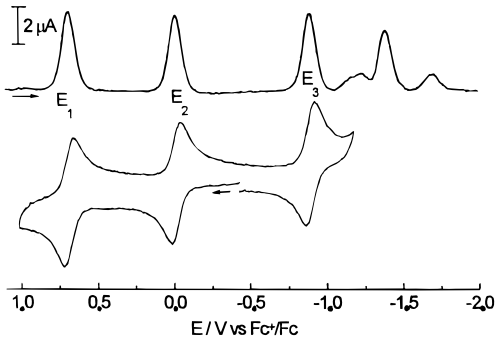

Figure 1. Cyclic and square-wave voltammograms of **1** in CH_3CN (0.10 M $[N(n\text{-}Bu)_4]PF_6$); glassy carbon electrode, scan rate of CV 200 mV s^{-1}; square-wave voltammogram: frequency 10 Hz, pulse height 25 mV.

Scheme 1. Valence Bond Description Using a Delocalized Model Which Leads to the Observed $S_{t,max} = 2$ for $[LFeCr^{III}FeL]^{2+}$ and $S_{t,max} = 1$ Ground State for $[LFeFeFeL]^{2+}$ According to Ref 12

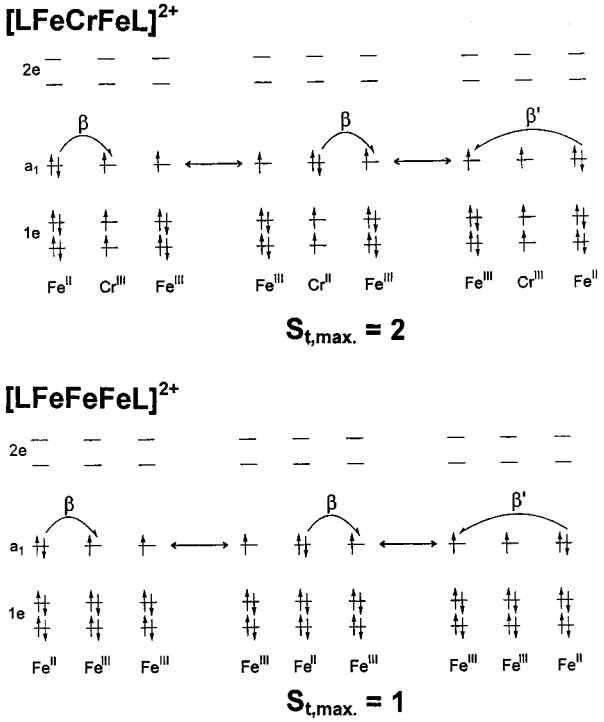

The cyclic voltammograms (CV) of **1**, **2**, and **3** are identical; that of **1** in CH_3CN (0.10 M $[N(n\text{-}Bu)_4]PF_6$) is shown in Figure 1. Three reversible one-electron transfer processes are clearly observed at $E^1{}_{1/2} = 0.69$ V vs ferrocenium/ferrocene (Fc^+/Fc), $E^2{}_{1/2} = -0.02$ V vs Fc^+/Fc, and $E^3{}_{1/2} = -0.90$ V vs Fc^+/Fc, which are assigned as depicted in eq 1. At −1.39 V vs Fc^+/Fc

$$[LFeNiFeL]^{4+} \underset{-e}{\overset{E^1+e}{\rightleftharpoons}} [LFeNiFeL]^{3+} \underset{-e}{\overset{E^2+e}{\rightleftharpoons}} [LFeNiFeL]^{2+} \underset{-e}{\overset{E^3+e}{\rightleftharpoons}} [LFeNiFeL]^{+} \quad (1)$$

the monocation $[LFeNiFeL]^+$ is irreversibly reduced with

(9) Papaefthymiou, V.; Girerd, J.-J.; Moura, I.; Moura, J. J. G.; Münck, E. *J. Am. Chem. Soc.* **1987**, *109*, 4703.
(10) Belinskii, M. I. *Mol. Phys.* **1987**, *60*, 793.
(11) (a) Borrás-Almenar, J. J.; Coronado, E.; Tsukerblat, B. S.; Georges, R. In *Molecular Magnetism: From Molecular Assemblies to the Devices*; Coronado, E., Ed.; Kluwer: Dordrecht, The Netherlands, 1996; p 105. (b) Borrás-Almenar, J. J.; Clemente, J. M.; Coronado, E.; Palii, A. V.; Tsukerblat, B. S.; Georges, R. *J. Chem. Phys.* **1996**, *105*, 6892.
(12) Glaser, T.; Beissel, T.; Bill, E.; Weyhermüller, T.; Schünemann, V.; Meyer-Klaucke, W.; Trautwein, A. X.; Wieghardt, K. *J. Am. Chem. Soc.*, in press.
(13) Beissel, T.; Birkelbach, F.; Bill, E.; Glaser, T.; Kesting, F.; Krebs, C.; Weyhermüller, T.; Wieghardt, K.; Butzlaff, C.; Trautwein, A. X. *J. Am. Chem. Soc.* **1996**, *118*, 12376.
(14) Beissel, T.; Bürger, K. S.; Voigt, G.; Wieghardt, K.; Butzlaff, C.; Trautwein, A. X. *Inorg. Chem.* **1993**, *32*, 124.

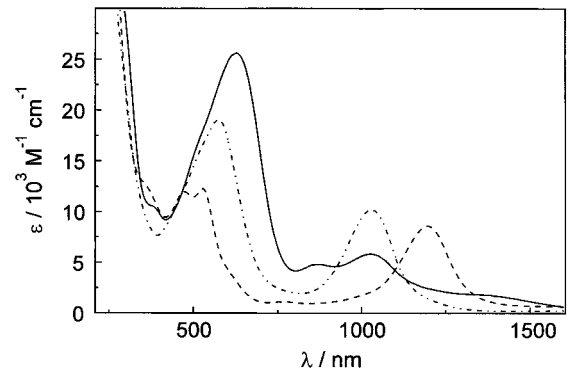

Figure 2. Electronic spectra of **1** (- - -), **2** (—·—), and **3** (—) in CH_3CN at 295 K.

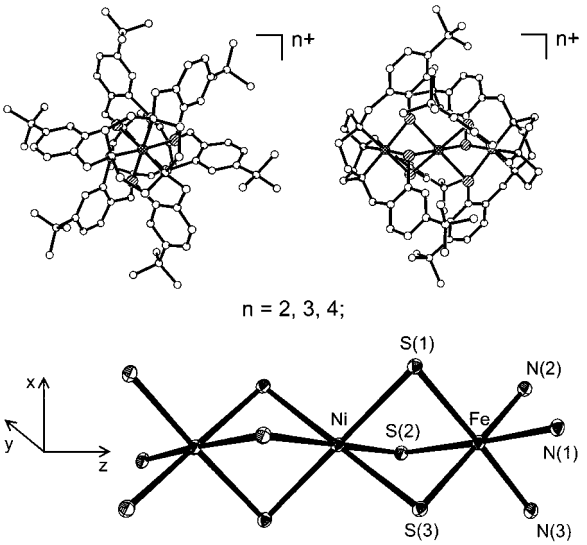

Figure 3. Structure of dication in crystals of $[LFeNiFeL](ClO_4)_2 \cdot 5CH_3CN$ (**1***). Top left: view down the Fe−Ni−Fe axis. Top right: side view. Bottom: metal ions with their donor atoms. The structure of the trication in **2*** is similar and not shown. The thermal vibrational ellipsoids of atoms are drawn at the 40% level.

formation of $[LFe^{II}]$.[14] Reduction of the dication is only reversible on the time scale of a CV experiment; it decomposes upon coulometry at −1.0 V vs Fc^+/Fc.

The electronic spectra of **1**, **2**, and **3** are shown in Figure 2. They are dominated by very intense ($>10^3$ L mol^{-1} cm^{-1}) transitions in the visible and near-infrared.

Single crystals of $[LFeNiFeL](ClO_4)_2 \cdot 5CH_3CN$ (**1***) suitable for X-ray crystallography were obtained by slow evaporation of the solvent from an acetonitrile solution of **2** which is slowly reduced under these conditions. Single crystals of $[LFeNiFeL](ClO_4)_3 \cdot 8$ acetone (**2***) were grown from an acetone solution of **2** at −40 °C. Figure 3 displays the structure of the dication in crystals of **1***; that of the trication in **2*** is similar and not shown. Both cations consist of three face-sharing thiolato-bridged octahedra with two terminal iron ions and a central nickel ion. The stereochemistry of these trinuclear cations, $[\{LM^1\}_2M^2]^{n+}$, has been discussed previously.[13] Only the staggered configuration of the six tertiary butyl groups (looking down the Fe···Ni···Fe axis) in the achiral stereoisomer $\Delta(\lambda\lambda\lambda)\cdots\Lambda(\delta\delta\delta)$ yields a stable, sterically not crowded structure. Thus only this isomer forms in solution. The di- and the trications possess idealized S_6 symmetry or D_{3d} considering the donor atoms of the respective first coordination sphere only. The iron ions have local C_{3v} symmetry (*cis*-N_3S_3 donor set) whereas the central nickel ion is in an octahedral environment comprising six bridging sulfur atoms both in **1*** and in **2***.

Table 1. Selected Bond Distances [Å] and Angles [deg] for 1* and 2*

	1*	2*		1*	2*
Fe−N1	2.036(3)	2.038(2)	Fe−S1	2.245(1)	2.2478(9)
Fe−N2	2.031(3)	2.042(2)	Fe−S2	2.243(1)	2.2459(9)
Fe−N3	2.038(3)	2.041(2)	Fe−S3	2.248(1)	2.2427(8)
Fe···Ni	3.054(1)	3.002(1)			
Ni−S1	2.345(1)	2.3395(8)	Ni−S1−Fe	83.38(4)	81.73(3)
Ni−S2	2.349(1)	2.3346(7)	Ni−S2−Fe	83.35(4)	81.88(3)
Ni−S3	2.359(1)	2.3144(10)	Ni−S3−Fe	83.02(4)	82.40(3)

Table 1 summarizes selected bond distances and angles. The three crystallographically independent Fe−N and Fe−S distances are within experimental error identical in **1*** and **2*** at 2.04 and 2.25 Å, respectively. These distances are also identical with those measured by EXAFS spectroscopy for **3** (see below). Thus oxidation of **1** to **2** and further to **3** does not affect the structural parameters at the terminal iron ions. In contrast, the average Ni−S bond distance at 2.35 Å in **1**, 2.33 Å in **2**, and 2.31 Å in **3** (EXAFS) appears to decrease with increasing oxidation level, although this effect is barely significant. Interestingly, in $[\{Co^{III}(aet)_3\}_2Ni^{II}]Cl_2 \cdot 3H_2O$,[16] a species with localized valencies and, consequently, with a central Ni^{II} ion, the Ni−S distance at 2.400 Å is the longest (aet = aminoethanethiolate). We take this as a structural indication that the central nickel ion in **1** cannot be described as a simple Ni^{II} but shows some degree of a higher than +II oxidation state. The short Fe−N and Fe−S bonds are indicative of a low-spin configuration at the iron ions in an octahedral environment.

A further structural aspect is worth mentioning. The $Fe_t\cdots Ni_c$ distances in **1**, **2**, and **3** at 3.054(1), 3.002(1), and 2.93(1) Å (EXAFS), respectively, decrease significantly with increasing oxidation level. This effect has also been observed for the series $[LFeMFeL]^{n+}$ (M = Cr, Co; $n = 1-3$; and M = Fe, $n = 2, 3$).[12]

EXAFS and XANES Spectroscopy. We have measured the EXAFS spectra (extended X-ray absorption fine structure) of complexes **1**, **2**, and **3** at the Fe *and* Ni K-edges at ambient temperature, respectively. The results are summarized in Table 2. Figure 4 shows the experimental and fitted *k* and *R* space data.

The results obtained for **1** and **2** show that the Fe···Ni, Fe−N, Fe−S, and Ni−S distances are in very good agreement with those obtained by single-crystal X-ray crystallography. This calibration gives us confidence that the theoretical phases used are appropriate.[17] It is therefore significant that the bond distances Fe−N and Fe−S are within experimental error invariant in **1**, **2**, and **3**, respectively. In contrast, the Fe···Ni distance decreases with increasing oxidation level as stated above.

XAS as an element specific spectroscopy allows one to analyze the oxidation state of a given element in a coordination compound. The position and intensity of the resonances and, in particular, the energy of the absorption edge position (Table 3) are features which depend on the d^n configuration. We have determined the edge positions from the maximum of the first derivative of the data in the rising edge region.[18] Resonances from the 1s level into half-occupied and/or empty d orbitals

(15) Wieghardt, K.; Walz, W.; Nuber, B.; Weiss, J.; Ozarowski, A.; Stratemeier, H.; Reinen, D. *Inorg. Chem.* **1986**, *25*, 1650.
(16) Konno, T.; Okamoto, K.; Hidaka, J. *Acta Crystallogr.* **1993**, *C49*, 222.
(17) Zabinsky, S. I.; Reber, J. J.; Ankudinov, A.; Albers, R. C.; Eller, M. J. *Phys. Rev. B*, in press.

Table 2. EXAFS Analysis of **1**, **2**, and **3**

		1		**2**		**3**	
atom	no.	R, Å	$10^3\,\sigma^2$, Å^2	R, Å	$10^3\,\sigma^2$, Å^2	R, Å	$10^3\,\sigma^2$, Å^2
Ni K-edge							
S	6	2.359(8)	6.1(6)	2.325(3)	4.8(2)	2.308(4)	4.3(3)
Fe	2	3.06(1)	7(1)	3.01(1)	9(1)	2.93(1)	7(1)
ΔE_0, eV		8(1)		8.7(5)		8.5(7)	
Fe K-edge							
N	3	2.050(6)	2.8(4)	2.04(1)	3.5(9)	2.041(7)	3.0(6)
S	3	2.265(3)	3.5(2)	2.242(5)	2.8(4)	2.255(3)	2.5(2)
Ni	1	3.06(1)	7(1)	3.01(1)	9(1)	2.93(1)	7(1)
C	3	2.83(1)	5(1)	2.83(2)	5(2)	2.84(1)	6(1)
C	3	2.91(1)	5(1)	2.91(2)	5(2)	2.91(1)	6(1)
C	3	3.02(1)	5(1)	3.02(2)	5(2)	3.03(1)	6(1)
C	3	3.33(1)	5(1)	3.33(2)	5(2)	3.34(1)	6(1)
ΔE_0, eV		4.1(6)		4(1)		4.5(6)	

[a] Fit results from the simultaneous refinement of the Ni and Fe K-edge EXAFS data. For the Ni fine structure only the first shell (six S) and the two iron atoms in the second shell including multiple scattering were included. For the Fe fine structure three N and three S atoms of the first shell and one Ni and 12 C atoms of the second shell were included. For the C atoms only one distance parameter was allowed. The Debye−Waller factor for all C atoms was constrained to a single value. The amplitude reduction factor was fixed at 0.9.

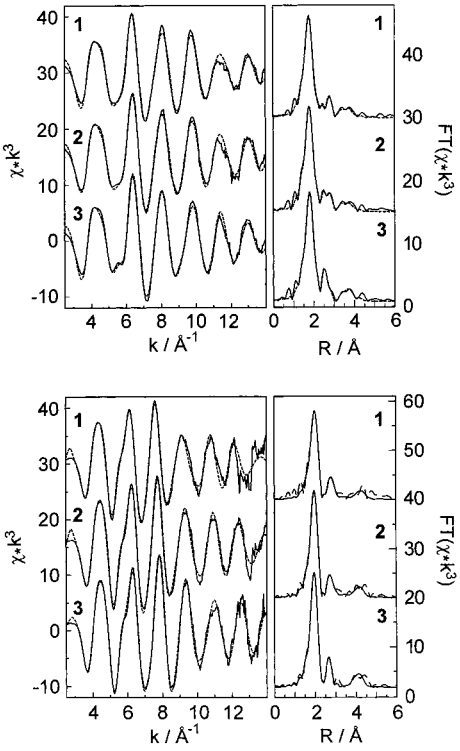

Figure 4. EXAFS spectra and fits of **1**, **2**, and **3** in k and R space. Top: Fe K-edge. Bottom: Ni K-edge.

Table 3. Fe and Ni K-Edge Positions

complex	Fe K-edge, eV	Ni K-edge, eV
1	7120.00(5)	8340.16(5)
2	7120.30(5)	8340.40(5)
3	7120.48(5)	8340.42(5)

give rise to distinct features superimposed on the K-edge transitions. We discuss these features in a qualitative fashion only.

The Fe K-edge XAS spectra of **1**, **2**, and **3** shown in Figure 5 display several well-resolved resonances at ∼7113 (pre-edge peak), 7120, 7126, and 7137 eV, respectively. Their exact

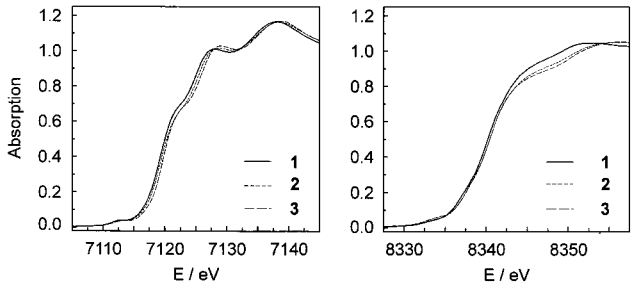

Figure 5. Fe (left) and Ni (right) K-edge XANES spectra of **1**, **2**, and **3**.

positions as well as the edge position depend on the oxidation level of the complexes. A change of the oxidation level going from **1** to **2** and **2** to **3** results in an upshift of ∼0.25 eV, respectively. This shift is significantly smaller than in the $[LFeMFeL]^{n+}$ ($M = Cr^{III}$, Co^{III}; $n = 1, 2, 3$) series where the central metal ion retains its +III oxidation state.[12] This is a clear indication that the one-electron oxidations in **1**, **2**, and **3** affect all *three* metal ions.

The Ni K-edge XAS spectra of **1**, **2**, and **3** show a very interesting feature. Whereas the shapes of the spectra of **2** and **3** are very similar and even their energy positions are identical, the spectrum of **1** is different both in shape and in energy position. An energy shift of 0.25 eV is observed on going from **1** to **2**. The shape of the Ni K-edge of **1** above 8342 eV is significantly different from those of **2** and **3**. This is in accord with the fact that the sign of the quadrupole splitting of the Mössbauer spectra changes from *negative* for **1** to *positive* for **2** and **3**, respectively (see below), indicating a significant change of the electronic structure at the iron and, consequently, also at the nickel ions in **1** as compared to **2** and **3**.

We also note that the Ni pre-edge peak of **3** is more intense than that of **2**. The transition probability for $1s \rightarrow e_g^*$ is inversely proportional to the number of electrons in the e_g^* orbitals. Therefore, the above intensity increase in **3** is due to a reduced occupancy of the e_g^* orbital, indicating some oxidation of the nickel ion on going from **2** to **3**.

In summary, the above Ni K-edge XAS data also clearly show that the one-electron oxidations **1** to **2** and **2** to **3** affect the electronic structure of the nickel ions in **1**, **2**, and **3**. Therefore, it is not possible to assign in the series $[LFeNiFeL]^{2+/3+/4+}$ localized oxidation states.

Mössbauer Spectroscopy. We have measured the zero-field Mössbauer spectra of **1**, **2**, and **3** at 4.2, 80, and 297 K,

(18) (a) Shadle, E. S.; Hedman, B.; Hodgson, K. O.; Solomon, E. I. *Inorg. Chem.* **1994**, *33*, 4235. (b) Shadle, E. S.; Hedman, B.; Hodgson, K. O.; Solomon, E. I. *J. Am. Chem. Soc.* **1995**, *117*, 2259. (c) Westre, T. E.; Kennepohl, P.; DeWitt, J. G.; Hedman, B.; Hodgson, K. O.; Solomon, E. I. *J. Am. Chem. Soc.* **1997**, *119*, 6297.

Table 4. Mössbauer Parameters of Complexes

complex	T, K	δ, mm s^{-1} [a]	ΔE_Q, mm s^{-1} [b]	Γ, mm s^{-1} [c]
1	4.2	0.38	−0.68	0.26
	80	0.38	−0.70	0.29
	297	0.28	−0.40	0.38
2	4.2	0.31	+0.52	0.44
	80	0.31	+0.52	0.36
	297	0.22	+0.42	0.28
3	4.2	0.26	+1.85	0.26
	80	0.25	+1.85	0.29

[a] Isomer shift vs α-Fe at 295 K. [b] Quadrupole splitting. The asymmetry parameter η was fixed to zero. [c] Full-width at half-height.

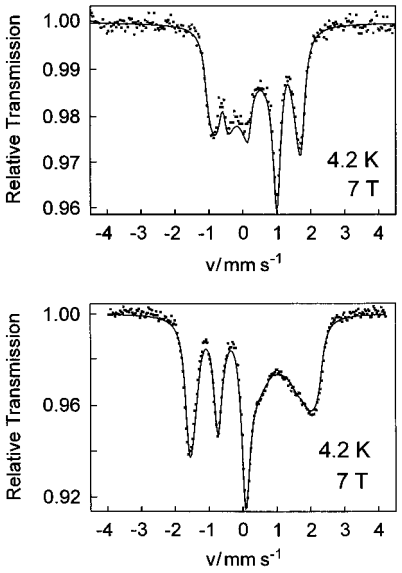

Figure 6. Mössbauer spectrum of **1** (top) and **3** (bottom) in an applied magnetic field of 7 T at 4.2 K. The fit was obtained using the parameters listed in Table 4 with a *negative* quadrupole splitting for **1** and a *positive* quadrupole splitting for **3**.

respectively. The results are summarized in Table 4. Each zero-field spectrum displays a single quadrupole doublet indicating the equivalence of the two terminal iron ions on the Mössbauer time scale (10^{-7} s). In a recent publication[12] we had established that the isostructural complexes $[LFe^{III}Co^{III}Fe^{III}L]^{3+}$ and $[LFe^{III}Cr^{III}Fe^{III}L]^{3+}$ containing localized valencies (low-spin Fe^{III}) show an isomer shift in the range 0.31−0.33 mm s^{-1} and a quadrupole splitting 1.85−2.00 mm s^{-1} at 4.2 K. These results do not agree well with the data for **1** and **2** in Table 4. From this we conclude again that it is not possible to a priori assign localized oxidation states to the individual metal ion in **1**, **2**, or **3**.

As we will show below, **1** has an $S_t = 0$, **2** an $S_t = {}^1/_2$, and **3** an $S_t = 0$ ground state. Mössbauer spectra of **1** and **3** measured at 4.2 K in an applied magnetic field of 7.0 T shown in Figure 6 confirm the diamagnetic ground state, respectively. The spectra were readily fitted with the parameters in Table 4 and without internal field by using a Hamiltonian described in detail in ref 12. Interestingly, the sign of the quadrupole splitting is found to be *negative* for **1** but *positive* for **3**.

Figure 7 displays the Mössbauer spectra of **2** ($S_t = {}^1/_2$) recorded in applied magnetic fields of 3.5, 5.0, and 7.0 T and at 1.5, 4.2, 8.0, and 120 K. From simulations for the well-isolated $S_t = {}^1/_2$ ground state in the slow relaxation limit the following hyperfine parameters were obtained: $(A_{xx}, A_{yy}, A_{zz})/\mu_N g_N = (4.92, 4.92, -5.37)$ T and $A^{iso}/\mu_N g_N = +1.49$ T using g values (fixed) from EPR spectra. The quadrupole splitting, ΔE_Q, is *positive*. The isotropic part of the **A** tensor, A^{iso}, for the $S_t = {}^1/_2$ ground state of **2** is also *positive*. In a simple

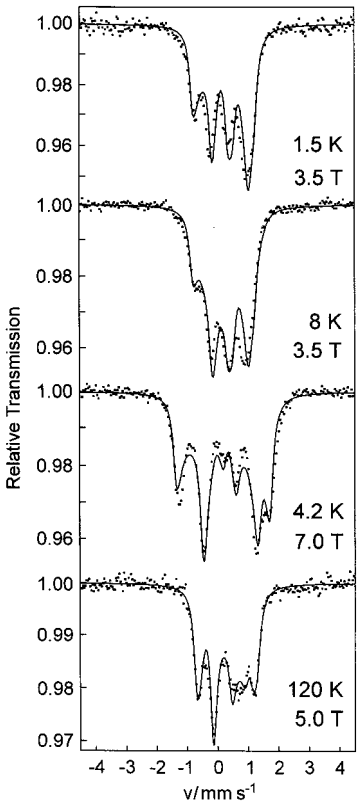

Figure 7. Variable-field, variable-temperature Mössbauer spectra of **2**. The fits were obtained using parameters given in the text and Table 4. The quadrupole splitting, ΔE_Q, is *positive*.

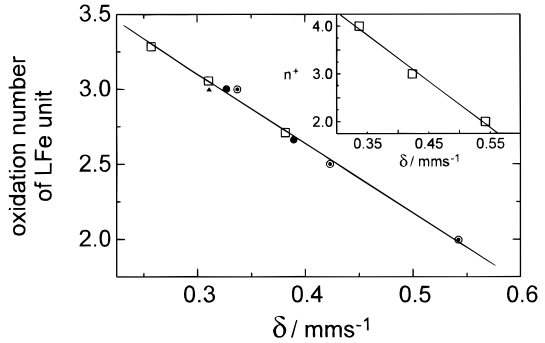

Figure 8. Dependence of the isomer shift, δ, of trinuclear complelxes $[LFeMFeL]^{n+}$ on the oxidation state and (inset) on the charge $n+$ of complexes: (⊙)$[LFeCr^{III}FeL]^{1+/2+/3+}$; (▲) $[LFe^{III}Co^{III}Fe^{III}L]^{3+}$; (●) $[LFe^{III}Fe^{III}Fe^{III}L]^{3+}$, $[LFe^{2.67}Fe^{2.67}Fe^{2.67}L]^{2+/3+}$; (□) $[LFeNiFeL]^{2+/3+/4+}$.

localized description with antiferromagnetic coupling between ls $Fe^{III}(\uparrow)$ ls $Ni^{III}(\downarrow)$ ls $Fe^{III}(\uparrow)$ the local spins at the iron ions would be oriented in the direction of the resulting total spin ($S_t = {}^1/_2$) and the sign of the A^{iso} tensor should be *negative*. We take this observation as further spectroscopic evidence that a localized model for **2** is not appropriate. On the other hand, we can at present not offer a rationale as to how the observed, positive sign of A^{iso} is achieved in a delocalized model because the vector coupling mechanism is more complicated.

It is interesting that the isomer shift, δ, of **1**, **2**, and **3** decreases linearly with increasing charge n+ within the trinuclear series as is shown in the inset of Figure 8. In the previous series $[LFeCr^{III}FeL]^{1+/2+/3+}$ and $[LFeCo^{III}FeL]^{3+}$ we have shown by XANES spectroscopy at the Cr and Co K-edges that the central metal ion Cr or Co possesses an oxidation state of +III irrespective of the charge $n+$ of the trinuclear species. Thus the iron ions in the monocation are low-spin Fe^{II}, in the dications

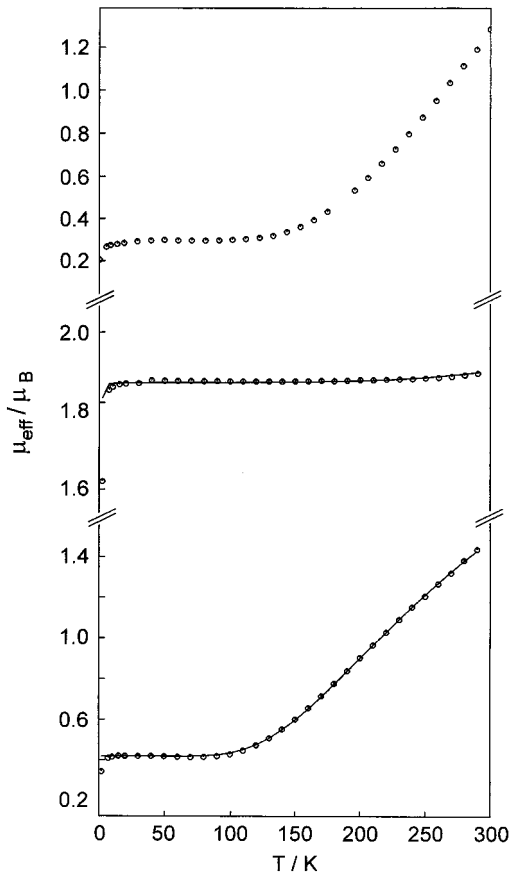

Figure 9. Temperature dependence of the effective magnetic moments of **1** (top), **2** (middle), and **3** (bottom). The fits were obtained by procedures described in the text.

mixed-valent 2.5, and the trications contain two low-spin ferric ions. As shown in Figure 8 the isomer shift δ of these complexes increases linearly with decreasing oxidation number of the iron ions. It is therefore possible to assign fractional oxidation numbers to the iron ions in the di-, tri-, and tetracation in **1**, **2**, and **3** if we assume that the above correlation holds for these species. For **1** an oxidation state distribution of $[LFe^{2.7}Ni^{2.6}Fe^{2.7}L]^{2+}$ prevails, for **2** it is $[LFe^{3.0}Ni^{3.0}Fe^{3.0}L]^{3+}$, and for **3** a distribution of $[LFe^{3.3}Ni^{3.4}Fe^{3.3}L]^{4+}$ is found. These data nicely agree with the XANES data (see above), which also indicate that one-electron oxidations going from the di- to the tri- and tetracations involves all *three* metal ions (two iron *and* the nickel ion). Interestingly, for **2** an even oxidation state of +III for each metal ion is experimentally determined.

Magnetic Susceptibility and EPR Spectroscopy. Temperature-dependent magnetic susceptibility measurements were performed on a SQUID magnetometer. The raw data were corrected for underlying diamagnetism by using Pascal's tabulated constants. Temperature-independent paramagnetism,[19] χ_{TIP}, is a fit parameter.

Figure 9 shows the effective magnetic moments calculated per trinuclear unit as a function of the temperature. For complex **1** the magnetic moment of 0.3 μ_B is temperature-independent in the range 20−120 K. At higher temperatures μ_{eff} increases to 1.32 μ_B at 295 K. This behavior is typical for an $S_t = 0$ ground state with a small amount of a paramagnetic impurity (0.2%; $S = {}^5/_2$). We attempted to model the above temperature dependence by using a localized valence description for **1** as $[ls\ Fe^{III}\ hs\ Ni^{II}\ ls\ Fe^{III}]^{2+}$ ($S_1 = S_3 = {}^1/_2$; $S_2 = 1$) with a spin Hamiltonian which includes coupling between adjacent Fe···Ni ions, $J_a = J_{12} = J_{23}$, and between the terminal iron ions, $J_t = J_{13}$. To reduce the number of parameters we assumed physically reasonable local values $g_{Fe} = 2.1$ and $g_{Ni} = 2.2$. The fit of the $\chi_M{\cdot}T$ values produced $J_a = -350\ cm^{-1}$ and $J_t = -347\ cm^{-1}$, but the resulting fit is not satisfactory. The measured magnetization in the temperature range 150−300 K rises significantly faster than it has been possible to model using a Heisenberg, Dirac, van Vleck (HDvV) operator. The HDvV Hamiltonian for the above spin system included only the system spin states $|0,1\rangle$, $|1,0\rangle$, $|1,1\rangle$, and $|2,1\rangle$ using Kambe's notation.[20] The energy spacing of these states depends on the coupling constants J_t and J_a as follows: $E(|0,1\rangle) = 0$, $E(|1,1\rangle) = 2J_a$, $E(|2,1\rangle) = 6J_a$, $E(|1,0\rangle) = 4J_a - 2J_t$. The experimentally determined singlet ground state of **1** requires a negative J_a (antiferromagnetic coupling). Further, it is natural to assume that $|J_a| > |J_t|$ considering the fact that adjacent metal ions are ~3 Å apart whereas it is ~6 Å for the two terminal iron ions. The marked increase of μ_{eff} at $T > 150$ K is then determined by the energy difference between the ground $|0,1\rangle$ and first excited state $|1,1\rangle$ which is independent of J_t. This increase cannot be modeled satisfactorily by two triplet states only, even in the physically meaningless limit of their degeneracy ($J_t = J_a$). This in turn means that the HDvV operator (i.e., a localized model) is not adequate. The transfer term in a double-exchange operator increases the number of spin states[10,11] and, in principle, allows a better fit.

The effective magnetic moment of **2** is constant at 1.87 μ_B in the range 50−200 K. It increases slightly to 1.89 μ_B at 295 K and decreases below 50 K due to weak intermolecular interactions to 1.62 μ_B at 2 K. It is possible to fit the data using a localized model, $[ls\ Fe^{III}\ ls\ Ni^{III}\ ls\ Fe^{III}]^{3+}$ ($S_1 = S_3 = {}^1/_2$; $S_2 = {}^1/_2$). With parameters $J_a = -390\ cm^{-1}$, $J_t = -220\ cm^{-1}$, $g_1 = g_3 = 2.17$, and $g_2 = 2.20$ an excellent fit has been achieved, but there are many other solutions possible. The data establish only that **2** has an $S_t = {}^1/_2$ ground state.

The data for **3** show that this complex possesses a diamagnetic ground state. Using the localized model $[ls\ Fe^{III}Ni^{IV}\ ls\ Fe^{III}]^{4+}$ with $S_1 = S_3 = {}^1/_2$ and $S_2 = 0$ we calculate an antiferromagnetic coupling constant $J_t = -270\ cm^{-1}$ and a g value of 2.33 ($\chi_{TIP} = 570 \times 10^{-6}\ cm^3\ mol^{-1}$; p.i. ($S = {}^5/_2$) = 0.5%). The fit is shown in Figure 9. Again, although the fit is reasonable, we doubt that the localized model is adequate.

The X-band EPR spectrum of **2** in frozen acetonitrile at 10 K is shown in Figure 10. An axial signal $S_t = {}^1/_2$ with $g_\perp = 2.409$ and $g_\parallel = 1.8$ ($g^{iso} = 2.23$) is the main component. A second signal (~1% intensity) with $g_\perp = 2.23$ and $g_\parallel = 2.06$ is reproducibly present. We do not know the origin of this signal as it is not a decomposition product of **2**.

Discussion

The terminal iron ions in a *fac*-N_3S_3 coordination sphere have local C_{3v} symmetry where the *z*-axis is directed along the trigonal Fe−M−Fe axis and the *x*,*y*-axes are oriented as shown in Figure 3. The t_{2g} orbitals in O_h symmetry are split into a doubly degenerate orbital set (1e in C_{3v}) and a nondegenerate a_1 orbital which corresponds to a d_{z^2} metal orbital. The $e(t_{2g})$ orbitals are π orbitals with respect to the metal−ligand bonds, and the $e(e_g)$ orbitals are of σ-type.

In a trigonal ligand field two directions of the splitting are possible, yielding an ordering of the ground state t_{2g} derived

(19) χ_{TIP}: **1**, $460 \times 10^{-6}\ mol^{-1}\ cm^3$; **2**, $730 \times 10^{-6}\ mol^{-1}\ cm^3$; and **3**, $570 \times 10^{-6}\ mol^{-1}\ cm^3$. These values are in the same range, $530-870 \times 10^{-6}\ mol^{-1}\ cm^3$, as observed for $[LFeMFeL]^{n+}$ (M = Cr, Co, Fe).[12]

(20) Kambe, K. *J. Phys. Soc. Jpn.* **1950**, *5*, 48.

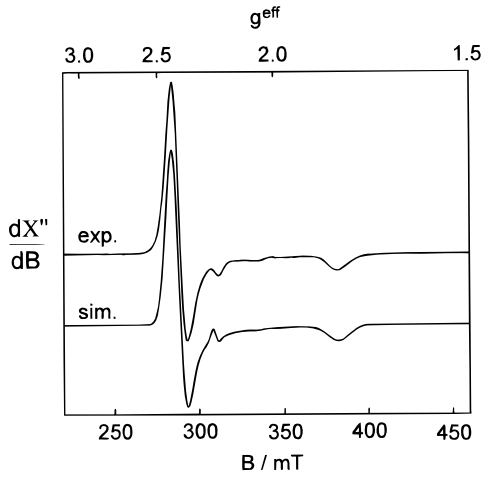

Figure 10. X-band EPR spectrum of **2** in frozen CH_3CN at 10 K. Experimental conditions: frequency 9.6455 GHz; power 100 μW, modulation amplitude 11.4 G; modulation frequency 100 kHz. The simulation was performed with Gaussian line shapes, $\Gamma = (111, 111, 176)$ G with 99.2% and $\Gamma = (45, 45, 80)$ G with 0.8%.

orbitals of $a_1$1e or 1ea_1. Experimentally, the sign of the quadrupole splitting parameter, ΔE_Q, of the Mössbauer spectra directly allows one to distinguish between these two possibilities. The valence electron contribution to the electric field gradient $(EFG)_{val}$ can be estimated by a simple ligand field consideration because the expectation values for the $(EFG)_{val}$ tensor elements are known for the individual metal d orbitals.[21] For a low-spin d^5 system there are two possible electron configurations in trigonal symmetry: $(1e)^4(a_1)^1$ and $(a_1)^2(1e)^3$ leading to $V_{zz} = (+4/7)e\langle r^{-3}\rangle$ and $V_{zz} = (-2/7)e\langle r^{-3}\rangle$, respectively.[22] Therefore, the experimentally determined sign of the quadrupole splitting yields the respective electron configuration: it is $(a_1)^2(1e)^3$ in **1** and $(1e)^4(a_1)^1$ in **2** and **3**.

The isomer shift of the Mössbauer spectrum of **1** in conjunction with the XANES spectra clearly indicates that the equivalent two iron ions have an oxidation state of approximately 2.7, which renders the central nickel ion 2.6. Thus in contrast to a localized model the ferric ions are somewhat reduced whereas the nickel(II) ion is oxidized: a distribution of $[LFe^{2.7}Ni^{2.6}Fe^{2.7}L]^{2+}$ is best in accord with the combined spectroscopic data. Thus **1** must be considered a mixed-valence compound (class III according to Robin and Day[2]).

Using a valence bond description with a series of resonance structures for the two possible ground states for **1**, namely, $S_t = 0$ *or* $S_t = 2$, shown in Figure 11 it is immediately evident that delocalization via a double-exchange mechanism stabilizes the *diamagnetic* ground state. There are three resonance structures involving Fe^{II},Fe^{III} and Ni^{II},Ni^{III} for the $S_t = 0$ state which are interrelated by symmetry-allowed one-electron transfer steps and none for the $S_t = 2$ state. Thus we are dealing with the first well-characterized example where a double-exchange mechanism over three metal ions stabilizes a diamagnetic ground state; i.e., the singlet over the quintet ground state. This behavior has been theoretically predicted by Belinskii.[10,11] Note that in *dinuclear* complexes containing only two paramagnetic centers double exchange always stabilizes the ground state with the highest possible spin multiplicity.[5−7]

The isomer shift of 0.31 mm s^{-1} measured for **2** is characteristic of two equivalent low-spin ferric ions which

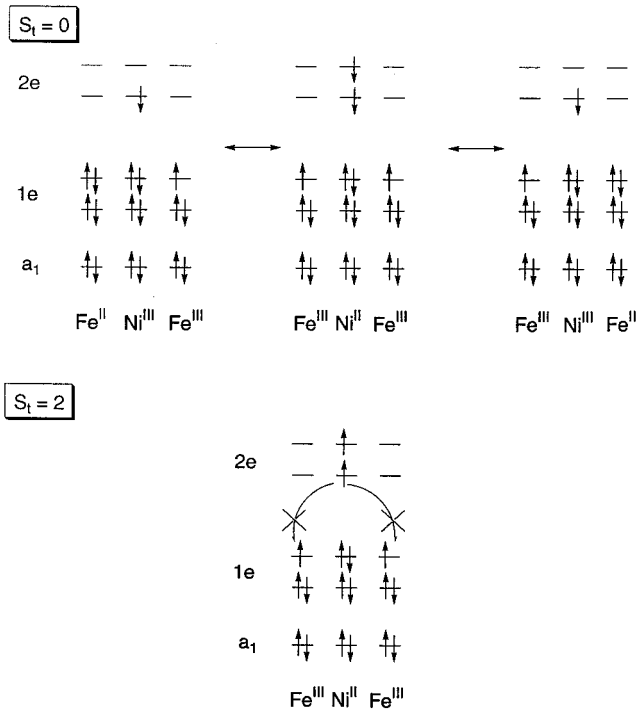

Figure 11. Resonance structures for **1** with $S_t = 0$ or $S_t = 2$ ground state. The orbital energy levels of the central metal ion are arbitrarily drawn equal to those of the terminal ions.

renders the central metal ion a nickel(III): [ls Fe^{III} ls Ni^{III} ls Fe^{III}] but in comparison to $[LFe^{III}Co^{III}Fe^{III}L]^{3+}$ the slightly smaller isomer shift of **2** does indicate some Fe^{IV} rather than Fe^{II} character in **2**. Since the quadrupole splitting is positive, a $(1e)^4(a_1)^1$ electron configuration for the ferric ions prevails. In accord with the XANES spectra, which clearly show that one-electron oxidations in the series **1**, **2**, and **3** affect the electronic structure of all three metal ions, we propose that in **2** also a delocalized model represents an adequate description. Figure 12 shows that the double-exchange mechanism stabilizes the $S_t = {}^1/_2$ over the $S_t = {}^3/_2$ ground state. Note that again the lower spin multiplicity state represents the ground state. Electron transfer from an a_1 to the 2e orbitals (and vice versa) is symmetry forbidden because they are orthogonal and, consequently, there is no overlap. Electron transfer is only possible between the 1e and 2e orbitals. The three resonance structures in Figure 12 do not possess the same weight; those involving Fe^{IV} contribute less to the ground state than the resonance structure involving $Fe^{III}Ni^{III}Fe^{III}$. Alignment of spins in **2** results in resonance structures with excited local states which affect delocalization unfavorably due to loss of spin polarization energy.[7a] Thus in the $S_t = {}^3/_2$ state electron transfer of a spin-down electron yields an electronically excited nickel(II), and similarly, transfer of a spin-up electron results in an excited Fe^{IV} ion. Complex **2** is therefore another example where the double-exchange mechanism (delocalization over three metal ions) stabilizes a ground state with the lowest possible spin multiplicity.

Complex **3** may be described in a first approximation as a $[LFe^{III}Ni^{IV}Fe^{III}L]^{4+}$ with localized oxidation states. From the positive quadrupole splitting parameter the $(1e)^4(a_1)^1$ electron configuration of the two equivalent ferric ions follows. As shown above it is possible to model the temperature dependence of the magnetic susceptibility data by using a localized model. The usual spin Hamiltonian $H = -2JS_1 \cdot S_2$ ($S_1 = S_2 = {}^1/_2$) yields then a very strong antiferromagnetic coupling constant of -270 cm^{-1}. On the other hand, the small isomer shift of 0.26 mm

(21) (a) Trautwein, A. X.; Bill, E.; Bominaar, E. L.; Winkler, H. *Struct. Bonding* **1991**, *78*, 1. (b) Gütlich, P. In *Mössbauer Spectroscopy*; Gonser, U., Ed.; Springer: Berlin, Heidelberg, New York, 1975.

(22) Bossek, U.; Nühlen, D.; Bill, E.; Glaser, T.; Wieghardt, K.; Trautwein, A. X. *Inorg. Chem.* **1997**, *36*, 2834.

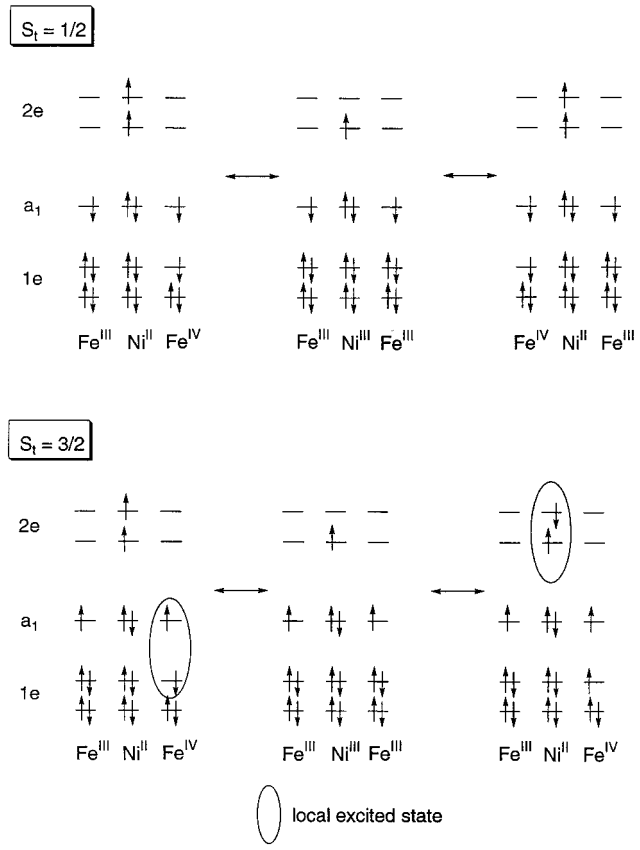

Figure 12. Resonance structures for **2** with $S_t = {}^1/_2$ or $S_t = {}^3/_2$.

s^{-1} is a clear indication that this localized model is incorrect because there is significant Fe^{IV} character observed for the iron ions. Using the relation in Figure 8 an oxidation state of 3.3 is deduced, which yields an average oxidation state of 3.3 at the nickel ion; i.e., **3** should be described as mixed-valent $[LFe^{3.3}Ni^{3.3}Fe^{3.3}L]^{4+}$.

It is interesting that in this case construction of resonance structures involving Fe^{III}, Fe^{IV}, Ni^{II}, Ni^{III}, and Ni^{IV} ions does not allow one to discern which of the two possible states, namely, $S_t = 0$ or $S_t = 1$, is the ground state. Figure 13 shows that symmetry-allowed one-electron transfer steps between adjacent metal ions (1e $\rightarrow$ 2e), the β pathway, produce five resonance structures stabilizing an $S_t = 1$ ground state. When one considers also one-electron transfer steps between the terminal iron ions ($a_1 \rightarrow a_1$), the β' pathway, spin alignment of the two a_1 magnetic orbitals results, leading to an $S = 0$ ground state. Otherwise electron transfer would yield a Pauli forbidden state.

Electron transfer via the β pathway between adjacent metal ions and delocalization via the 1e $\rightarrow$ 2e orbitals (double exchange) stabilizes an $S_t = 1$ ground state whereas the β' pathway favors an $S = 0$ ground state. Thus the ratio β/β' determines the actual ground state in **3**. Schematically this is shown in Figure 14. A significant contribution to the stabilization of the $S = 0$ ground state in **3** originates from the resonance integral β' between two terminal $S_i = {}^1/_2$ spins (superexchange).

In other words, complete delocalization over three metal ions via the β pathway favors an $S_t = 1$ ground state. This has been shown to be the case for $[LFeFeFeL]^{2+}$ which is isoelectronic with **3**. On the other hand, $[LFe^{III}Co^{III}Fe^{III}L]^{3+}$ has been shown to also possess an $S_t = 1$ ground state. The excited singlet state lies 83 cm^{-1} above the triplet ground state. Here a localized description has been inferred from Mössbauer spectroscopy. The

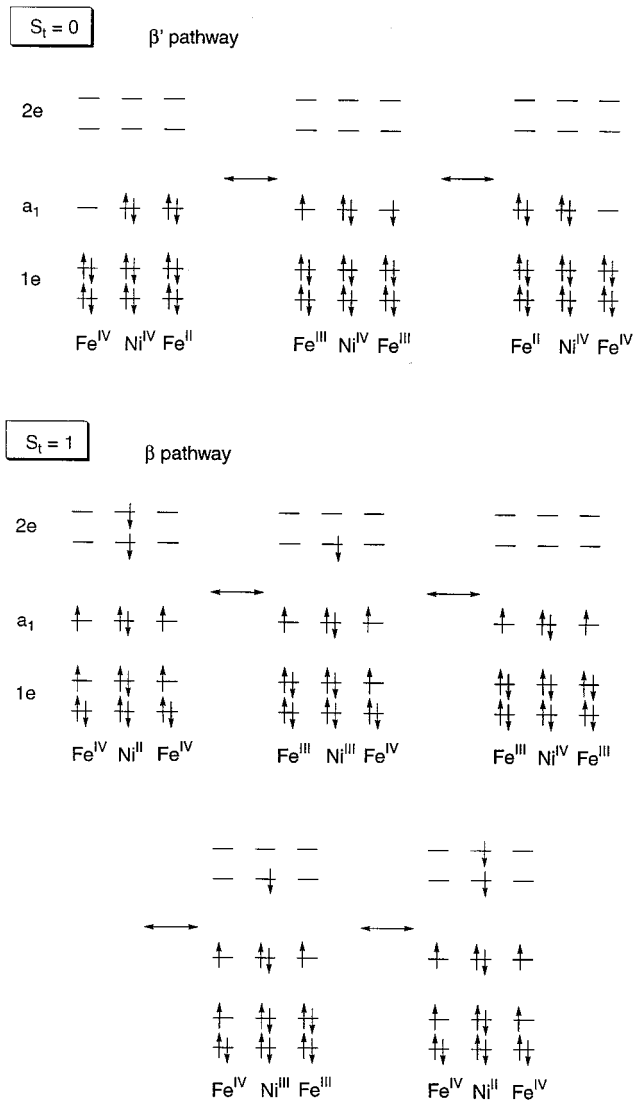

Figure 13. Resonance structures for **3** emphasizing one-electron transfer steps between (top) terminal metal ions (β' pathway) and (bottom) adjacent ions (β pathway).

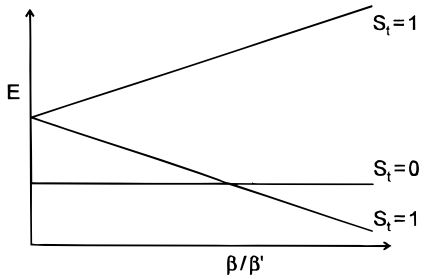

Figure 14. Schematic qualitative representation of the effect of the interplay between electron exchange interactions between the terminal ls Fe^{III} ions in **3** (β' pathway) and one-electron transfer from ls Fe^{III} to Ni^{IV} (β pathway), in terms of the ratio β/β', on the energy of the $S_t = 0$ and the $S_t = 1$ ground state.

singlet ground state of **3** lies ~500 cm^{-1} below the excited triplet state. Thus the absolute energy gap of the singlet−triplet states in the two isoelectronic complexes **3** and $[LFe^{III}Co^{III}Fe^{III}L]^{3+}$ is rather small and the β/β' ratio must be quite similar for both species but on either side of the crossover point shown in Figure 14. We cannot at present correlate in a simple fashion this fact with structural parameters of these complexes. Detailed MO calculations on both species are called for.

Table 5. Crystallographic Data of Complexes

complex	**1**·5acetonitrile	**2**·8acetone
empirical formula	$C_{88}H_{123}Cl_2Fe_2N_{11}NiO_8S_6$	$C_{102}H_{156}Cl_3Fe_2N_6NiO_{20}S_6$
fw	1896.64	2255.45
space group	$P\bar{1}$	$P\bar{1}$
a, Å	13.065(2)	13.155(2)
b, Å	13.626(3)	14.747(2)
c, Å	14.043(3)	16.237(3)
α, deg	114.47(3)	114.20(2)
β, deg	97.67(3)	96.57(2)
γ, deg	90.34(3)	98.86(2)
V, Å	2249.9(9)	2783.2(8)
Z	1	1
T, K	100(2)	100(2)
radiation *λ*, Å	0.710 73	0.710 73
ρ calcd, g cm^{-3}	1.400	1.346
μ(Mo Kα), cm^{-1}	7.85	6.76
diffractometer	CAD4	Siemens SMART CCD
R1[a] [$I > 2\sigma(I)$]	0.055	0.052
wR2[b] [$I > 2\sigma(I)$]	0.140	0.126

[a] $R1 = \sum||F_o| - |F_c||/\sum|F_o|$, $R_w = [\sum w(|F_o| - |F_c|)^2/\sum wF_o^2]^{1/2}$ where $w = 4F_o^2/\sigma^2(F_o^2)$. [b] $wR2 = [\sum[w(F_o^2 - F_c^2)^2]/\sum[w(F_o^2)^2]]^{1/2}$ where $w = 1/\sigma^2(F_o^2) + (aP)^2 + bP$, $P = (F_o^2 + 2F_c^2)/3$.

Conclusion

The preparation and structural characterization of three isostructural heterotrinuclear complexes containing the dication $[\{LFe\}_2Ni]^{2+}$ in **1**, the trication $[\{LFe\}_2Ni]^{3+}$ in **2**, and the tetracation $[\{LFe\}_2Ni]^{4+}$ in **3** have been achieved. Their respective electronic ground states have been determined by a combination of spectroscopic and magnetochemical methods.

The most important result is the observation that the description of the electronic structures using the concept of localized oxidation states at the metal ions (e.g., Fe^{III}, Ni^{II}, Ni^{III}, Ni^{IV}) is not appropriate for—at least—**1** and **3** and probably also for **2**. Fe and Ni metal K-edge X-ray absorption spectroscopy most clearly demonstrates that the one-electron oxidation of **1** to **2** and **2** to **3** affects *all three* metal ions simultaneously. The iron ions are equivalent in all three compounds.

In a delocalized model the observed minimum spin multiplicity of the ground state is attained in all three species ($S_t = 0$ in **1**, $S_t = {}^1/_2$ in **2**, and $S_t = 0$ in **3**) via a double-exchange mechanism. This is the first time that this effect has been experimentally observed for trinuclear complexes. It had been theoretically predicted.[10,11]

Experimental Section

The starting complex $[Fe^{III}L]$ has been prepared as described previously.[14]

CAUTION. *Perchlorate salts are potentially explosive and should only be prepared in small quantities and handled with appropriate precautions.*

[LFeNiFeL](PF$_6$)$_2$ (1). To an Ar-flushed solution of [LFe] (0.37 g; 0.52 mmol) in methanol (50 mL) was added $NiCl_2 \cdot 6H_2O$ (0.61 g; 2.6 mmol). The solution was heated to reflux for 1 h, whereupon the color changed from blue-green to red. To the cooled (20 °C) solution was added (dropwise) a methanol (20 mL) solution of $NaPF_6$ (0.5 g). After standing for 15 h at ambient temperature black-red crystals of **1** were collected by filtration. Yield: 0.30 g (65%). Electrospray ionization mass spectrometry (ESI) (CH_3CN) *m*/*z* (relative intensity): 716.5 $\{[LFe]^+$, 52$\}$, 746.4 $\{[LFeNiFeL]^{2+}$, 100$\}$, 774.4 $\{[LFeNi]^+$, 32$\}$, 1638.5 $\{[LFeNiFeL](PF_6)^+$, 9$\}$. Anal. Calcd for $C_{78}H_{108}N_6S_6P_2F_{12}Fe_2Ni$: C, 52.56; H, 6.11; N, 4.71; S, 10.79. Found: C, 52.9; H, 6.4; N, 4.8; S, 11.0.

[LFeNiFeL](ClO$_4$)$_3$ (2). To an Ar-flushed solution of **1** (0.12 g; 0.067 mmol) in acetone (25 mL) was added $[Ni^{III}(tacn)_2](ClO_4)_3$15 (0.05 g; 0.074 mmol). After stirring of the solution for 30 min at room temperature a color change from red to violet was observed. To the filtered solution was added $NaClO_4$ (0.20 g) dissolved in acetone (10 mL). After standing for 15 h at ambient temperature the black microcrystalline precipitate was collected by filtration. Yield: 0.08 g (66%). Anal. Calcd for $C_{78}H_{108}N_6S_6Cl_3O_{12}Fe_2Ni$: C, 52.31; H, 6.08; N, 4.69; S, 10.74. Found: C, 52.0; H, 6.4; N, 4.5; S, 10.4.

[LFeNiFeL](PF$_6$)$_4$ (3). To a mixture of **1** (0.12 g; 0.067 mmol) in methanol (50 mL) were added five drops of methanesulfonic acid and PbO_2 (0.07 g; 0.30 mmol). Within 10 min of stirring at room temperature a clear blue solution was obtained. After addition of a solution of $NaPF_6$ (0.50 g) in methanol (10 mL) a black precipitate formed within minutes. The material was collected by filtration and washed with a small amount of water and then diethyl ether. The solid material was stored at 77 K. Yield: 0.13 g (93%). Anal. Calcd for $C_{78}H_{108}N_6S_6P_4F_{24}Fe_2Ni$: C, 45.21; H, 5.25; N, 4.06; S, 9.28. Found: C, 44.9; H, 5.5; N, 4.1; S, 9.2.

X-ray Crystallographic Data Collection and Refinement of the Structures. Black single crystals of **1*** and **2*** selected directly from the mother liquor using glass fibers were fixed with a drop of perfluoropolyether. Immediate mounting on the diffractometer equipped with a cryogenic nitrogen cold stream prevented evaporation of solvent of crystallization. Graphite-monochromated Mo Kα radiation ($\lambda = 0.710\ 73$ Å) was used. Crystallographic data of the compounds and diffractometer types used are listed in Table 5. Cell constants for **1*** were obtained from a least-squares fit of the setting angles of 25 carefully centered reflections whereas a subset of 8192 stronger reflections was used for the determination of the unit cell constants of **2***. Intensity data were collected at −173(2) °C using the Θ−2Θ scan technique, and a hemisphere run taking frames at 0.30° in *ω* for **1*** and **2*** respectively. Data were corrected for Lorentz and polarization effects, but no absorption correction was carried out due to small absorption coefficients. The Siemens ShelXTL[23] software package was used for solution, refinement, and artwork of the structures. Both structures were readily solved and refined by direct methods and difference Fourier techniques performed on DEC Alpha workstations. Neutral atom scattering factors were obtained from tables.[24] All non-hydrogen atoms were refined anisotropically except those of disordered solvent

(23) ShelXTL V.5, Siemens Analytical X-ray Instruments, Inc., 1994.

molecules, which were isotropically refined. All hydrogen atoms were placed at calculated positions and refined as riding atoms with isotropic displacement parameters.

A perchlorate anion in **2*** was found to be disordered on a crystallographic inversion center yielding an arrangement of two edge-sharing tetrahedral parts with an occupancy of 0.5 for each oxygen. Split atom models were applied for acetonitrile solvent molecules in **1*** and an acetone molecule in **2*** which are disordered over two sites, respectively. With occupancy factors of 0.5 for these disordered atoms and 8 bond length restraints for N ≡ C (1.13 Å) and C−C (1.46 Å), a satisfactory model for the solvent channel in **1*** was obtained.

X-ray Absorption Spectroscopy (XAS). The XAS spectra were recorded at the beam lines E4 and X1.1 at HASYLAB (DESY, Hamburg, Germany). The beam lines are equipped with three ionization chambers, which allow a calibration of each spectrum according to a reference sample. The measurements were performed at room temperature. Monochromatization was achieved by a Si(111) monochromator for the Fe and Ni K-edges. At beam line E4 a focusing mirror was installed in front of the monochromator for further rejection of the harmonics. For the suppression of harmonics the monochromator was detuned to 50% of its peak intensity. Energy calibration was achieved by use of reference samples. For the Fe K-edge an α-Fe foil and for the Ni K-edge a Ni foil were chosen.

The energy calibration of the data was performed using WINXAS,[25] whereas the normalization and data reduction were done with EXPROG,[25] using a Victoreen function below the edge and three cubic splines above the edge. For the EXAFS analysis FEFF6/FEFFIT232[25] was used. The edge positions were defined as the maximum of the first derivative in the rising edge.

XAS as an element specific spectroscopy allows one to analyze the influence of the oxidation state on each element of a complex. XANES monitors this dependence by the position and intensity of the resonances as well as by the edge position. A change of the oxidation state results in a shift of the edge position. For samples with similar edge shapes, changes of the average oxidation state of the different metal atoms were readily deduced from a shift of the minimum of the second derivative in the rising edge.

The EXAFS signal depends on the radial distribution of the backscattering atoms around the absorbing atom. A single type of backscatterer at similar distances results in a smaller width of the distribution function as compared to two types at different bond distances. This has been observed for the first shell of the present samples where the terminal Fe atom is coordinated to three S and three N atoms whereas the central Ni ion is coordinated to six S atoms. Hence, one obtains in the Fourier transform of the Fe K-edge EXAFS a broad peak at a reduced radius of 1.8 Å and at the Ni K-edge a narrow peak at a reduced radius of 1.9 Å. Due to the different phase shifts, e.g., for nitrogen and sulfur backscattering atoms, typically the phase uncorrected distance distributions (Fourier transforms) are discussed. The much higher Fourier transform peak intensity in the Ni case is due to the higher degree of order, which is also reflected by a larger EXAFS amplitude.

Knowledge of the structure of **1*** and **2*** simplifies a detailed multiple-scattering EXAFS analysis. Considering only statistical reasons we would be able to optimize more than 20 parameters for each scan. To overcome the problem of high correlations between different parameters we have used the simplest model possible. For the Ni K-edge this includes only the contributions from the six sulfur atoms in the first shell, the backscattering from the neighboring iron atoms, the very important multiple scattering contributions for the Ni−S−Fe−S−Ni−Fe−M path, and even more importantly, the multiple scattering contributions within the first shell up to fourth order.

The local environment of the terminal iron atoms is not as symmetric as that of the central metal ion. Therefore, more parameters had to be included in the calculations. The first coordination sphere consists of sulfur and nitrogen atoms. The multiple scattering contributions within this shell are much smaller due to the lower symmetry compared to the central metal atom with its six sulfur ligands at similar distances. The larger average distances of these sulfur ligands result in a contribution of the multiple scattering within the first coordination sphere at 3.9 Å for the Ni K-edge, whereas the corresponding contribution for the Fe K-edge is at 3.7 Å. The fit of these peaks is not perfect because additional contributions from single scattering of several carbon atoms at distances >4 Å were not included in the refinement (carbon atoms of the macrocyclic ligand at ∼3 Å were).

The measurements on the terminal and central metal atoms contain the same information about the metal−metal distance and its disorder. Hence, this information can be extracted with much higher accuracy if both measurements are refined simultaneously. Thus we have used a multiple edge fit in the refinements, which implies the use of the same parameter for the Fe−Ni distance and its Debye−Waller parameter, respectively.

Physical Methods. Infrared spectra (400−4000 cm^{-1}) of solid samples were recorded on a Perkin-Elmer 2000 FT-IR spectrometer as KBr disks. UV−vis−near IR spectra of solutions were measured on a Perkin-Elmer Lambda 19 spectrophotometer in the range 210−3200 nm at ambient temperatures. Positive ion ESI mass spectra were obtained by using a Finnigan MAT95 or a HP5989 mass spectrometer. Cyclic voltammetric and coulometric measurements were performed on EG & G equipment (potentiostat/galvanostat model 273A) on Ar-flushed acetonitrile solutions of samples containing 0.10 M $[N(n\text{-}Bu)_4]PF_6$ as supporting electrolyte under an argon blanketing atmosphere. Temperature-dependent and magnetic field dependent magnetic susceptibilities of powdered samples were measured by using a SQUID magnetometer (Quantum Design) at 1.0, 4.0, and 7 T, respectively (2.0−300 K). For calculations of the molar magnetic susceptibility, χ_M, the experimental susceptibilities were corrected for the underlying diamagnetism of the sample by using tabulated Pascal's constants and for the temperature-independent paramagnetism (χ_{TIP}) which was obtained by a fitting procedure. EPR spectra of frozen solutions and powdered solids were recorded on a Bruker ESP 300E spectrometer equipped with a helium flow cryostat (X-band Oxford Instruments ESR 910; S-, Q-band Oxford Instruments CF935). The X-band resonator was a dual-mode cavity (Bruker ER4116DM/95). The Mössbauer spectra were recorded on an alternating constant-acceleration spectrometer. The minimal line width was 0.24 mm s^{-1} (full-width at half-height). The sample temperature was maintained constant either in an Oxford Variox or in an Oxford Mössbauer-Spectromag cryostat. The latter is a split-pair superconducting magnet system for applied fields

(24) *International Tables for X-ray Crystallography;* Kynoch Press: Birmingham, U.K., 1991.

(25) (a) Ressler, T.; LLNL, EXAFS program for Windows 3 Version 2.4. http://ourworld.compuserve.com/homepage/t ressler/. (b) Hermes, C.; Nolting, H. F. EMBL-Outstation Hamburg, Germany: *EXAFS data analysis and evaluation program package for PC.* (c) FEFF6: Zabinsky, S. I.; Rehr, J. J.; Ankudinov, A.; Albers, R. C.; Eller, M. J. Submitted to *Phys. Rev.* FEFIT232: Newville, M.; Ravel, B.; Huskel, D.; Stern, E. A.; Yacoby, Y. *Physica B* **1995**, *208−209*, 154.

up to 8 T where the temperature of the samples can be varied in the range 1.5−250 K. The field at the samples is oriented perpendicular to the γ-beam. The ^{57}Co/Rh source (1.8 GBq) was positioned at room temperature inside the gap of the magnet system at a zero-field position. Isomer shifts are referenced relative to α-iron metal at 295 K. Simulations of the Mössbauer spectra were performed by using the Hamiltonian described in more detail in ref 12.

Acknowledgment. We thank the Fonds der Chemischen Industrie and the German Federal Ministry of Education, Science, Research and Technology (BMBF) for financial support.

Supporting Information Available: Tables of crystallographic and crystal structure refinement data, atom coordinates, bond lengths and angles, anisotropic thermal parameters, and calculated positional parameters of hydrogen atoms for **1*** and **2***. This material is available free of charge via the Internet at http://pubs.acs.org.

IC9811289